# Bearing capacity of a sand layer on clay by finite element limit analysis

**J.S. Shiau, A.V. Lyamin, and S.W. Sloan**

**Abstract:** Rigorous plasticity solutions for the ultimate bearing capacity of a strip footing resting on a sand layer over clay soil are obtained by applying advanced upper and lower bound techniques. The study compares these solutions with other published results and investigates the effect of various strength and geometry parameters. Assuming the soil layers obey an associated flow rule, the results presented typically bound the collapse load to within ±10% or better.

*Key words:* limit analysis, bearing capacity, layered soils, finite elements.

**Résumé :** On a obtenu des solutions rigoureuses en plasticité pour la capacité portante ultime d'une semelle filante sur une couche de sable reposant sur un sol argileux en utilisant les techniques avancées de la limite supérieure et inférieure. L'étude compare ces solutions avec d'autres résultats publiés et examine l'effet de différents paramètres de résistance et de géométrie. En supposant que les couches de sol obéissent à une loi d'écoulement associé, les résultats ont présenté la charge de rupture typiquement limitée à l'intérieur de ±10 % ou mieux.

*Mots clés :* analyse limite, capacité cortante, sols en couches, éléments finis.

[Traduit par la Rédaction]

## Introduction

The need to determine the bearing capacity of a compacted sand or gravel layer on soft clay arises frequently in foundation engineering. Of the published approaches to this problem, the semi-empirical solutions of Meyerhof (1974) and Hanna and Meyerhof (1980) are perhaps the most widely used in practice. Their methods are also known as punching shear models, as they assume the sand layer to be in a state of passive failure along vertical planes beneath the footing edges. Another commonly used semi-empirical approach is the load spread model, in which the sand layer is assumed to merely spread the load to the underlying clay foundation (e.g., Terzaghi and Peck 1948; Houlsby et al. 1989). This technique ignores the shear strength of the sand and transforms the problem to the classical one of estimating the bearing capacity of a clay layer that is subjected to a surcharge.

A more rigorous approach, based on the upper bound theorem of limit analysis, has been used by Chen and Davidson (1973), Florkiewicz (1989), and Michalowski and Shi (1995) to calculate the bearing capacity of multilayered soils. These studies consider various rigid block mechanisms that, at the point of collapse, assume power is dissipated solely at the interfaces between adjacent blocks. After optimizing the geometry to furnish the minimum dissipated power, the mechanism that gives the lowest value is used to compute the best upper bound on the limit load. To give confidence in the accuracy of the solutions obtained from upper bound calculations, it is desirable to perform lower bound calculations in parallel so that the true result can be bracketed from above and below (Davis 1968; Chen 1975; Sloan 1988, 1989). Unfortunately, due to the difficulty in constructing statically admissible stress fields by traditional methods, this is rarely done in practice.

Although conventional finite element analysis can be used to predict the bearing capacity of multilayered soils (Griffiths 1982; Burd and Frydman 1997), the estimate so obtained is neither an upper bound nor a lower bound on the true value. Moreover, great care needs to be exercised with displacement finite element predictions in the fully plastic range, as the results can be very inaccurate due to the occurrence of locking (Nagtegaal et al. 1974; Sloan and Randolph 1982). This phenomenon, which is characterized by a constantly rising load–deformation response, occurs when the displacement field becomes overconstrained by the requirements of an incompressible plastic flow rule. To estimate undrained limit loads accurately using displacement finite elements in plane strain, it is prudent to avoid using low-order formulations (Sloan and Randolph 1982) unless they are used with some form of selective integration (Nagtegaal et al. 1974).

In this paper, we use finite element formulations of the limit analysis theorems to obtain rigorous plasticity solutions for the bearing capacity of a layer of sand on clay. Following Merifield et al. (1999), who considered the classical bearing capacity problem of a two-layered clay, we use the bounding methods to bracket the true solution from above and below. The techniques themselves have been developed only recently and are discussed in detail by Lyamin and Sloan

Received 30 April 2002. Accepted 10 April 2003. Published on the NRC Research Press Web site at http://cgj.nrc.ca on 8 September 2003.

**J.S. Shiau, A.V. Lyamin, and S.W. Sloan.**[1] Civil, Surveying and Environmental Engineering, University of Newcastle, Callaghan, NSW 2308, Australia.

[1]Corresponding author (e-mail: scott.sloan@newcastle.edu.au).

 doi: 10.1139/T03-042 

**Fig. 1.** Problem notation and potential failure mechanisms.

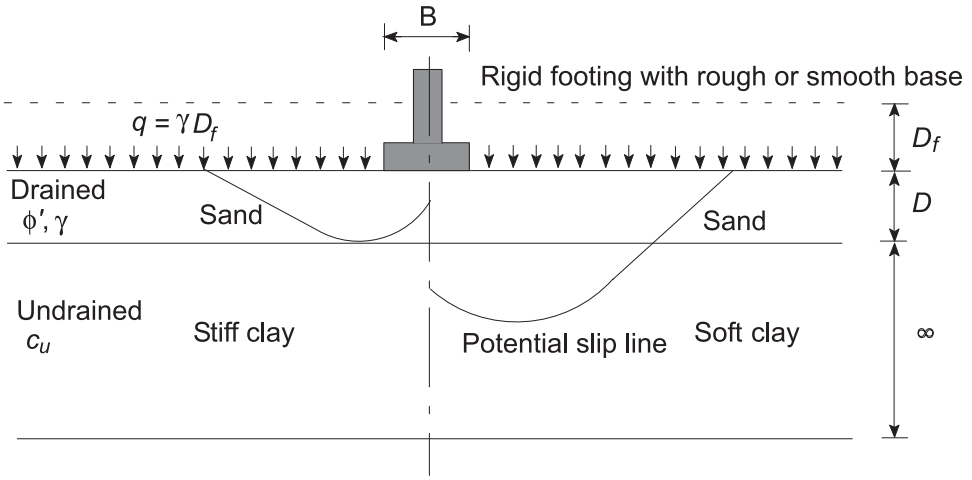


**Fig. 2.** Lower bound finite elements with linear stress fields.

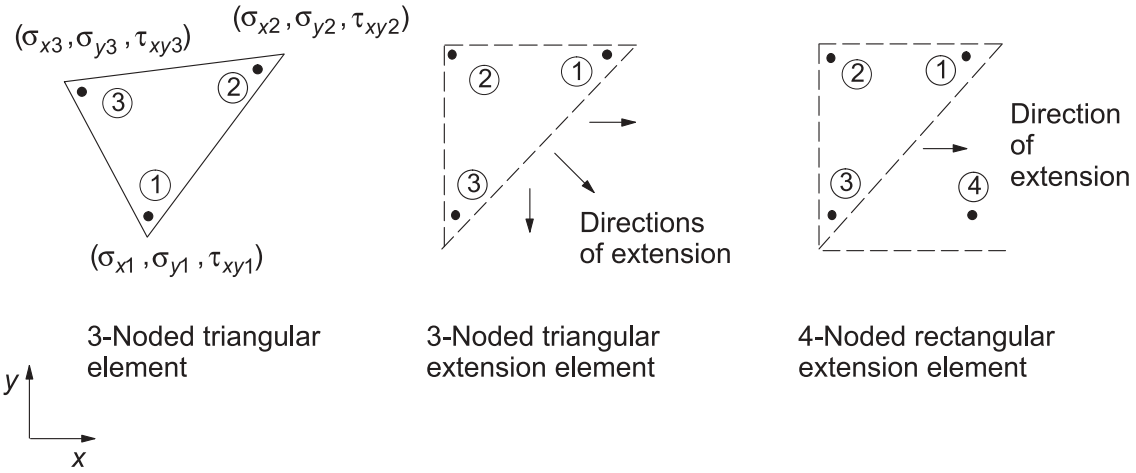


**Fig. 3.** Statically admissible stress discontinuity.

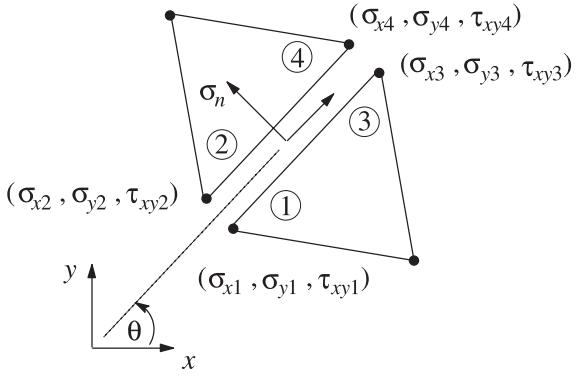


$$\sigma_n = \sigma_x \sin^2\theta + \sigma_y \cos^2\theta - \tau_{xy} \sin 2\theta$$

$$\tau = \frac{1}{2}(\sigma_y - \sigma_x) \sin 2\theta + \tau_{xy} \cos 2\theta$$

$$\sigma_{n1} = \sigma_{n2} \quad \tau_1 = \tau_2$$
$$\sigma_{n3} = \sigma_{n4} \quad \tau_3 = \tau_4$$

(2002*a*, 2002*b*). These procedures effectively supersede the earlier formulations proposed by Sloan (1988, 1989) and Sloan and Kleeman (1995) which, although successful in a wide range of practical applications, are less efficient.

## Problem definition

The bearing capacity problem considered in this paper is illustrated in Fig. 1. A strip footing of width $B$ rests on a sand layer that has a thickness $D$, an internal friction angle $\phi'$, a unit weight $\gamma$, and a surcharge $q$. The sand layer is underlain by a deep bed of clay that has an undrained shear strength $c_u$. Only short-term stability of the footing is considered, so the sand layer is assumed to be fully drained and the clay bed undrained.

Taken in isolation, the bearing capacity of the sand layer

**Fig. 4.** Mesh 1 for (*a*) lower bound and (*b*) upper bound analysis ($D/B$ = 1).

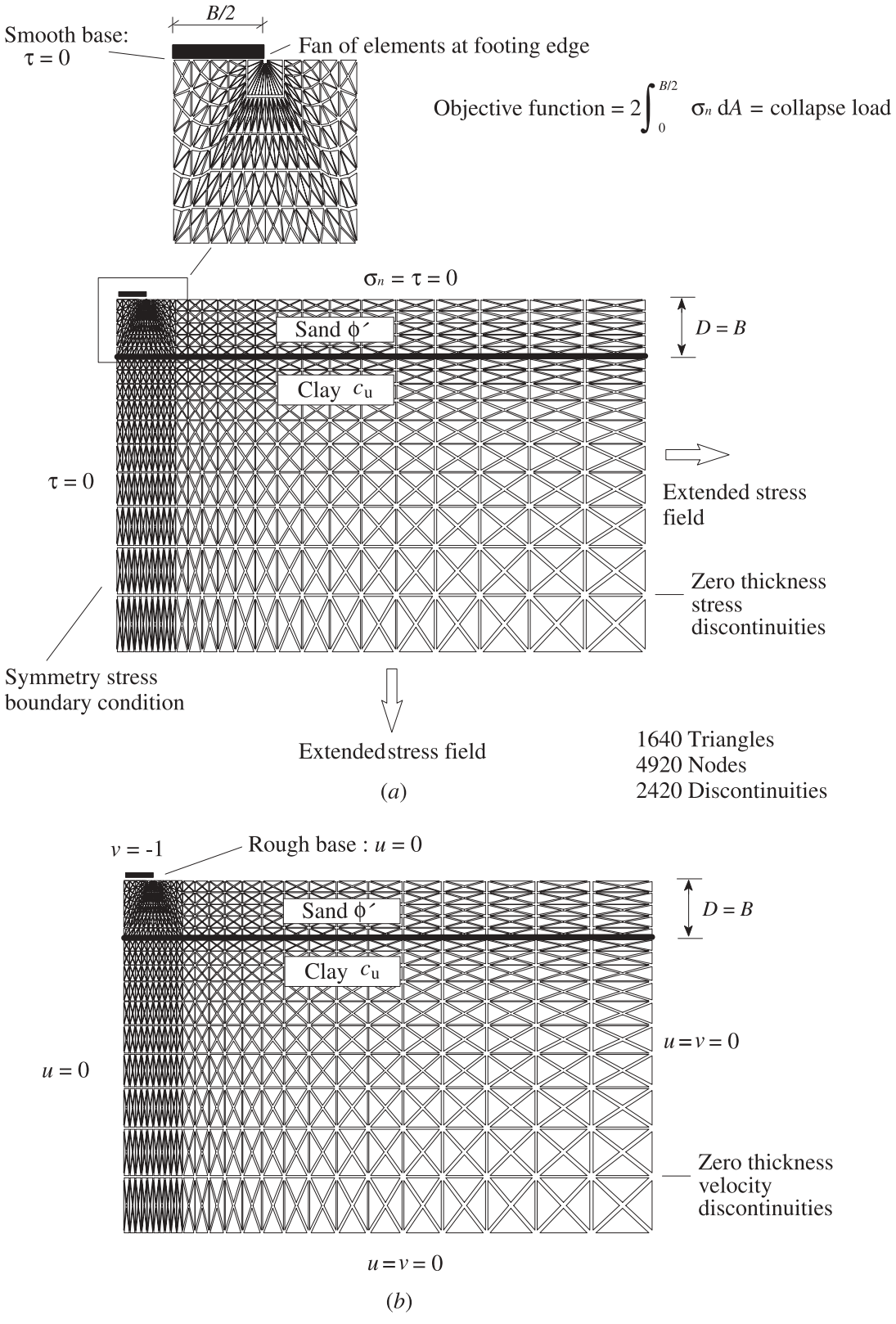

**Fig. 5.** Upper bound finite element with linear velocity field and constant stress field.

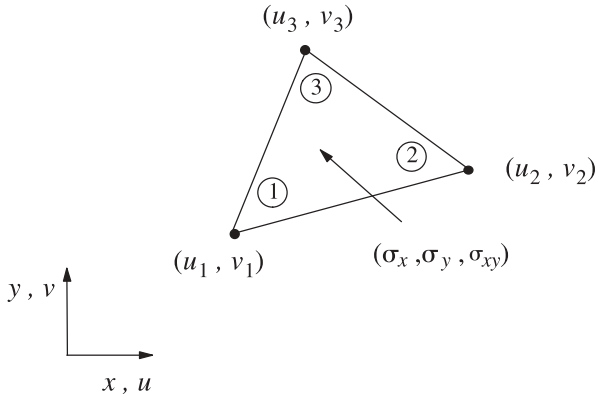


will be governed by $\phi'$, $\gamma$, and $q$, with other possible factors being the dilation angle $\psi'$ and the footing roughness. Classical limit analysis theory assumes an associated flow rule, where normality of the plastic strains to the yield function applies and the dilation angle is set equal to the friction angle. Allowing for the presence of the clay layer, and assuming associated flow with a perfectly rough footing, the ultimate bearing capacity of the two-layer foundation problem can be expressed in the dimensionless form

$$[1] \qquad \frac{p}{\gamma B} = f\left(\frac{D}{B}, \frac{c_u}{\gamma B}, \frac{q}{\gamma B}, \phi'\right)$$

where $p$ is the average limit pressure. Accordingly, in the following, the bearing capacities are presented in terms of the dimensionless quantities $D/B$, $c_u/\gamma B$, $q/\gamma B$, and $\phi'$, with the role of the dilation angle and footing roughness investigated separately.

## Numerical limit analysis models

This section gives a very brief summary of the finite element formulations of the upper and lower bound theorems. A more detailed description of the techniques, including a discussion of the solution algorithms used to solve the resulting optimization problem, can be found in Lyamin and Sloan (2002*a*, 2002*b*) and will not be repeated here.

The lower bound limit theorem states that if any equilibrium state of stress can be found which balances the applied loads and satisfies the yield criterion as well as the stress boundary conditions, then the body will not collapse (Chen 1975). Stress fields that satisfy these requirements, and thus give lower bounds, are said to be statically admissible. The key idea behind the lower bound analysis applied here is to model the stress field using finite elements and use the static admissibility constraints to express the unknown collapse load as a solution to a mathematical programming problem. For linear elements, the equilibrium and stress boundary conditions give rise to linear equality constraints on the nodal stresses, and the yield condition, which requires all stress points to lie inside or on the yield surface, gives rise to a nonlinear inequality constraint on each set of nodal stresses. The objective function, which is to be maximized, corresponds to the collapse load and is a function of the unknown stresses. For linear elements, this function is also linear. After all the element coefficients are assembled, the final optimization problem is thus one with a linear objective function, linear equality constraints, and nonlinear inequality constraints.

The lower bound formulation proposed by Lyamin and Sloan (2002*a*) handles both two- and three-dimensional stress fields and, in the former case, employs the linear elements shown in Fig. 2. Note that it incorporates statically admissible stress discontinuities at all interelement boundaries (Fig. 3) and special extension elements for completing the stress field in an unbounded domain (Fig. 2). Unlike displacement finite element meshes, each node is unique to a single element and several nodes may share the same coordinates. Although the stress discontinuities increase the total number of variables for a fixed mesh, they also introduce extra "degrees of freedom" in the stress field, thus improving the accuracy of the solution. Along a given discontinuity the normal and shear stresses must be continuous, but the tangential normal stress may be discontinuous.

As the formulation of Lyamin and Sloan (2002*a*) uses linear elements in both two and three dimensions, the objective function and equality constraints are linear in the unknowns. As discussed previously, the equality constraints arise because the stress field needs to satisfy equilibrium in the continuum and the discontinuities, as well as the stress boundary conditions. Some additional constraints may also be required to incorporate special types of loading along the domain boundaries. After assembling the various objective function coefficients and equality constraints for the mesh, and imposing the nonlinear yield inequalities on each node, the lower bound formulation of Lyamin and Sloan leads to a nonlinear programming problem of the form

$$[2] \qquad \begin{aligned} &\text{maximize} && \mathbf{c}^T\boldsymbol{\sigma} \\ &\text{subject to} && \mathbf{A}\boldsymbol{\sigma} = \mathbf{b} \\ & && f_i(\boldsymbol{\sigma}) \le 0 \quad i = \{1, \ldots N\} \end{aligned}$$

where $\mathbf{c}$ is a vector of objective function coefficients, $\boldsymbol{\sigma}$ is a vector of unknowns (nodal stresses and possibly element unit weights), $\mathbf{c}^T\boldsymbol{\sigma}$ is the collapse load, $\mathbf{A}$ is a matrix of equality constraint coefficients, $\mathbf{b}$ is a vector of coefficients, $f_i$ is the yield function for node $i$, and $N$ is the number of nodes. The solution to eq. [2], which constitutes a statically admissible stress field, can be found efficiently by solving the system of nonlinear equations that define its Kuhn-Tucker optimality conditions. Indeed, the two-stage quasi-Newton solver developed by Lyamin (1999) usually needs fewer than about 50 iterations, regardless of the problem size. Because it does not require the yield surface to be linearized, the formulation can be used for a wide range of convex yield criteria.

A "fan" mesh for a lower bound analysis of the problem defined in Fig. 1 is shown in Fig. 4*a*. The grid consists of 4920 nodes, 1640 triangular elements, and 2420 stress discontinuities. It includes special extension elements along the bottom and right boundaries (not shown for clarity) to extend the stress field throughout the semi-infinite domain. The fan of elements centred on the footing edge permits the principal stresses to rotate around this point and improves

**Fig. 6.** Kinematically admissible velocity discontinuity.

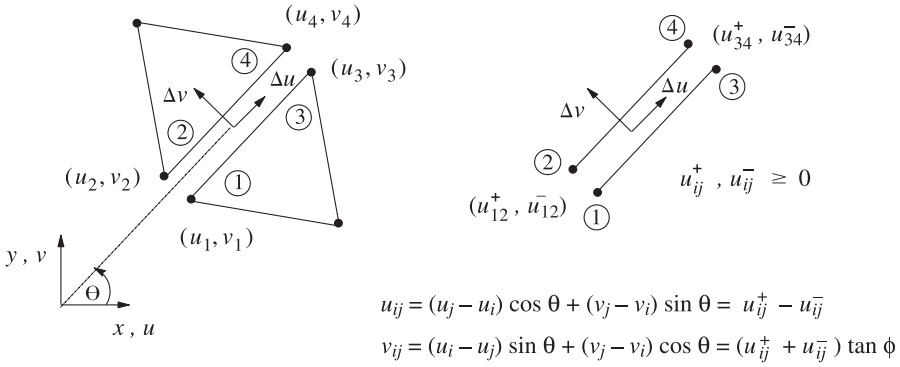


**Fig. 7.** Comparison of results.

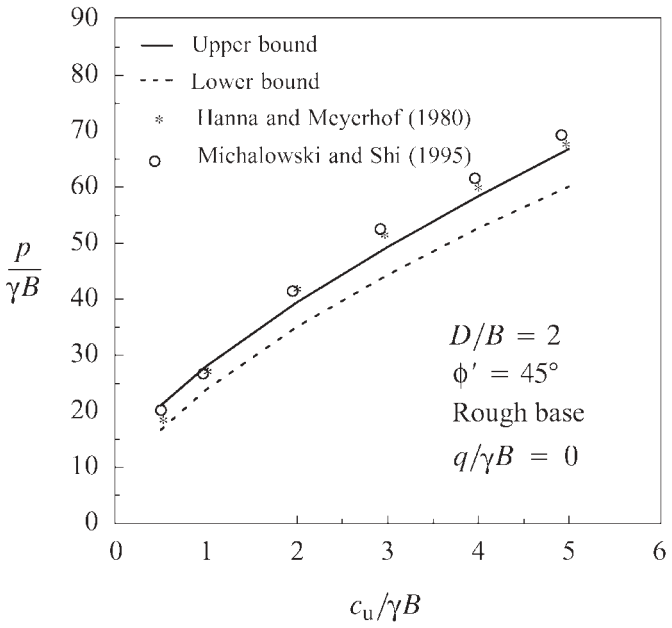


**Fig. 8.** Comparison of results.

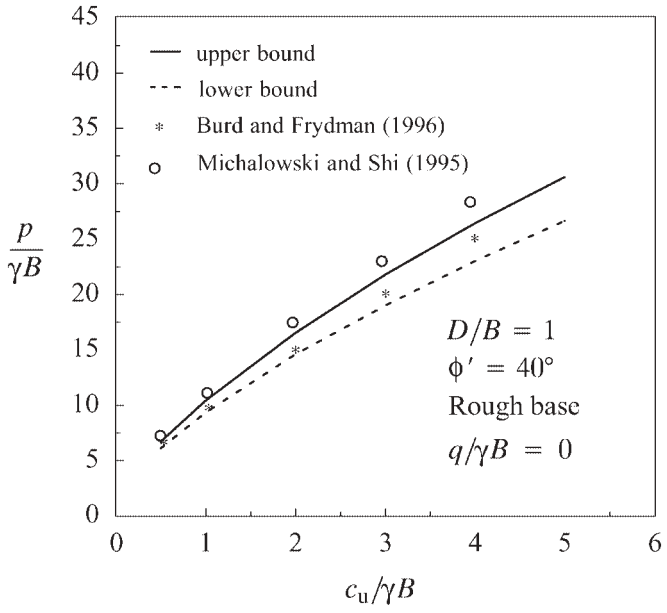


the accuracy of the lower bound. This aspect and the results from an alternative type of mesh are investigated in a later section of the paper.

To model a smooth footing that has no shear stress on its underside, additional constraints have to be imposed at all element nodes along the footing–soil interface. For a rough footing, the shear stress is typically nonzero and governed solely by the specified yield criterion.

The upper bound theorem can be formulated in terms of finite elements by adopting a similar approach to that just described for the static case. This theorem states that the power dissipated by any kinematically admissible velocity field can be equated to the power dissipated by the external loads to give a rigorous upper bound on the true limit load. A kinematically admissible velocity field is one that satisfies compatibility, the flow rule, and the velocity boundary conditions. In a finite element formulation of the upper bound theorem, the velocity field is modelled using appropriate variables, and the optimum (minimum) internal power dissipation is obtained as the solution to a mathematical programming problem.

**Fig. 9.** Effect of zero dilation angle.

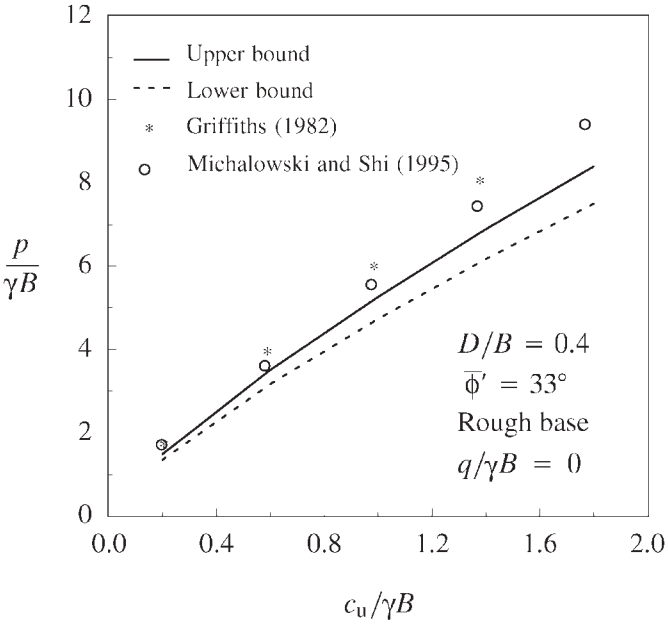

**Fig. 10.** Mesh 2 for (*a*) lower bound and (*b*) upper bound analysis (*D*/*B* = 0.5).

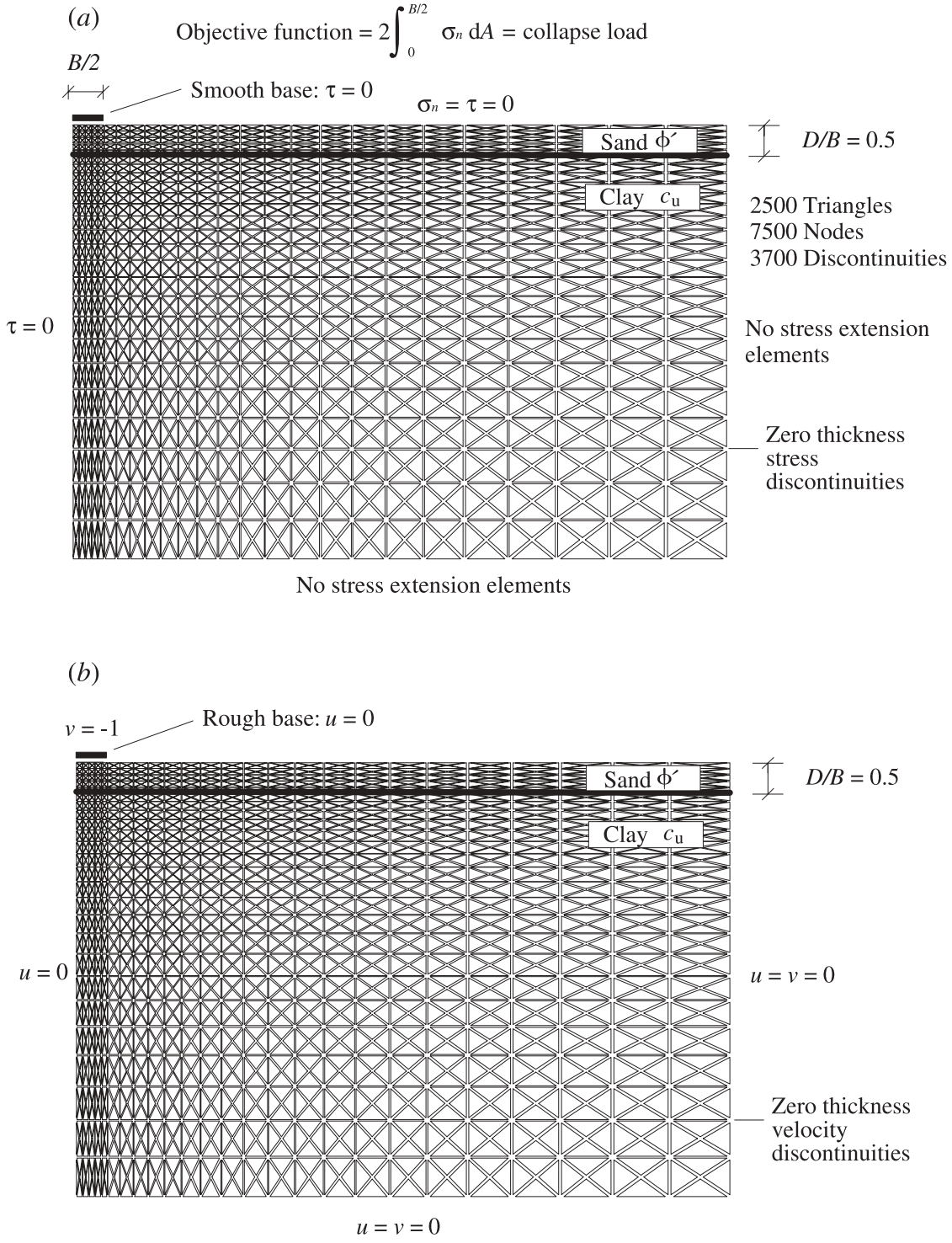


In the formulation of Lyamin and Sloan (2002*b*), the upper bound is found by the solution of a nonlinear programming problem. Their procedure uses linear triangles to model the velocity field, and each element is also associated with a constant stress field and a single plastic multiplier rate (Fig. 5). The element plastic multipliers do not need to be included explicitly as variables, however, even though they are used in the derivation of the formulation. This is because the final optimization problem can be cast in terms of the nodal velocities and element stresses alone. To ensure kinematic admissibility, flow-rule constraints are imposed on the nodal velocities, element plastic multipliers, and element stresses. In addition, the velocities are matched to the specified boundary conditions, the plastic multipliers are constrained to be non-negative, and the element stresses are constrained to satisfy the yield criterion. Following Sloan

**Table 1.** Effect of mesh arrangement on bearing capacity ($p/\gamma B$) for the case of $\phi' = 40°$, $D/B = 1$, and $q/\gamma B = 0$.

| | $p/\gamma B$ | | | | | |
|---|---|---|---|---|---|---|
| | Mesh 1 (Fig. 4) | | | Mesh 2 (Fig. 10) | | |
| $c_u/\gamma B$ | Lower bound (LB) | Upper bound (UB) | Accuracy (%)[a] | Lower bound (LB) | Upper bound (UB) | Accuracy (%)[a] |
| 0.5 | 6.01 (55) | 6.65 (34) | ±5.3 | 5.82 (110) | 6.68 (59) | ±7.4 |
| 1 | 9.26 (63) | 10.34 (36) | ±5.8 | 8.93 (125) | 10.37 (57) | ±8.1 |
| 2 | 14.50 (65) | 16.46 (37) | ±6.8 | 13.64 (156) | 16.50 (53) | ±10.5 |
| 3 | 18.96 (74) | 21.74 (43) | ±7.3 | 17.34 (182) | 21.84 (56) | ±12.9 |
| 4 | 22.96 (66) | 26.37 (44) | ±7.4 | 20.35 (169) | 26.61 (61) | ±15.4 |
| 5 | 26.59 (64) | 30.54 (39) | ±7.4 | 22.76 (216) | 30.86 (56) | ±17.8 |

**Note:** The values in parentheses are CPU time in seconds for a Pentium III 800 desktop personal computer.
[a]Accuracy determined as ±100(UB – LB)/(2 × LB).

**Fig. 11.** Bearing capacity of sand on clay for $D/B = 0.25$.

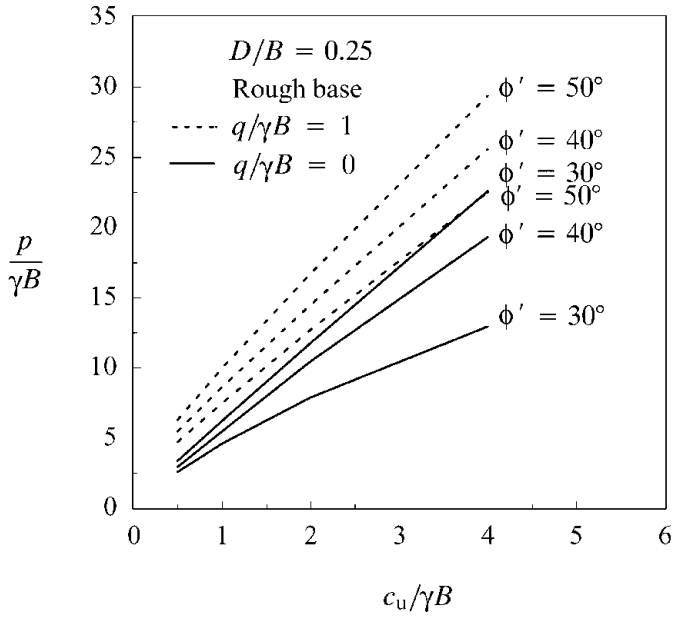


**Fig. 12.** Bearing capacity of sand on clay for $D/B = 0.5$.

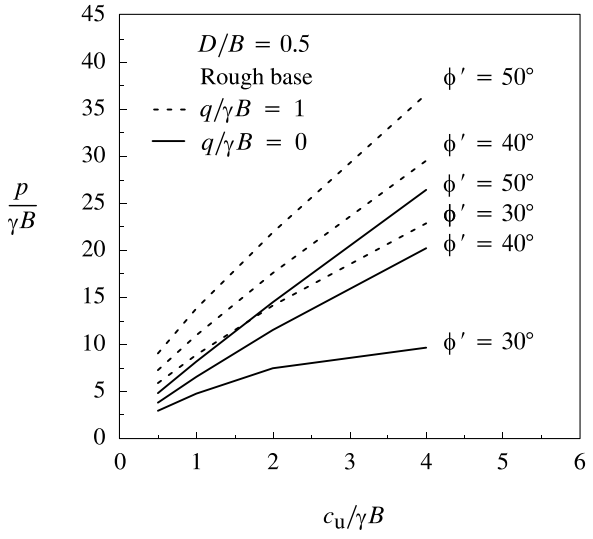


**Fig. 13.** Bearing capacity of sand on clay for $D/B = 1$.

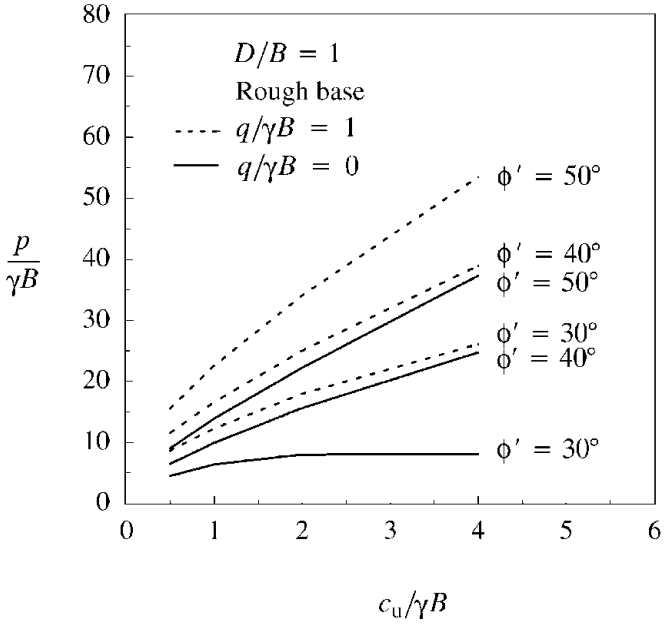


**Fig. 14.** Bearing capacity of sand on clay for $D/B = 2$.

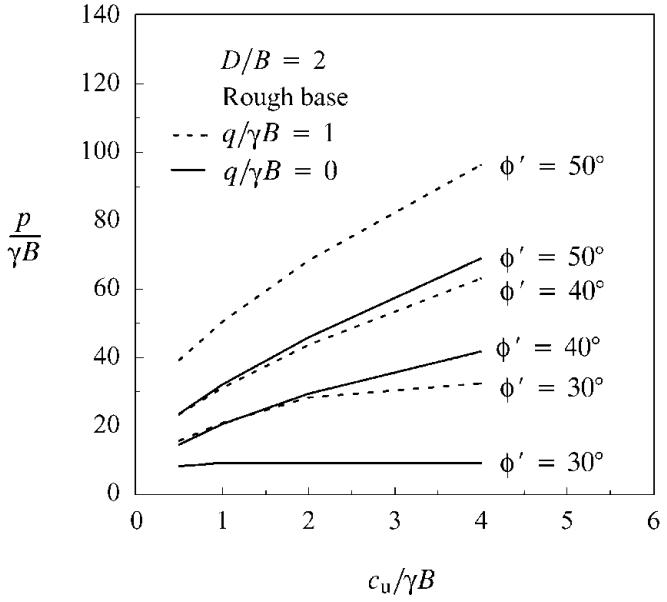

**Fig. 15.** Velocity diagrams for various values of $D/B$ ($\phi' = 30°$, $c_u/\gamma B = 1$, $q/\gamma B = 0$).

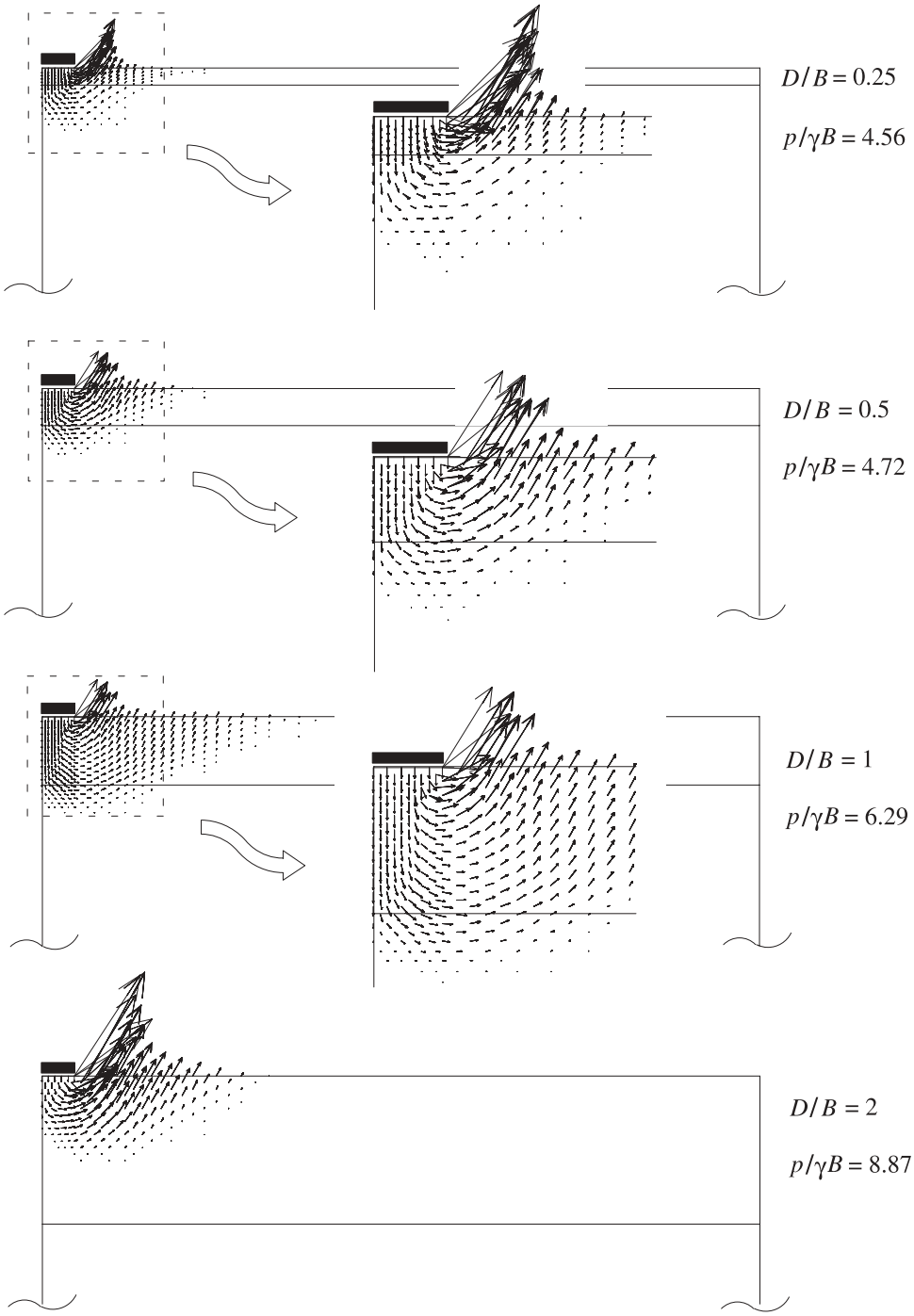


and Kleeman (1995), the method of Lyamin and Sloan permits velocity discontinuities at all interelement boundaries in the mesh. As shown in Fig. 6, each discontinuity is defined by four nodes and requires four unknowns to describe the velocity jumps along its length.

With the elements shown in Figs. 5 and 6, plastic deformation can occur in both the continuum and the velocity discontinuities, giving rise to two different sources of power dissipation. For a given set of prescribed velocities, the finite element formulation works by choosing the set of velocities and stresses that minimize the dissipated power. This power is then equated to the power dissipated by the external loads to yield a strict upper bound on the true limit load.

After assembling the various objective function coeffi-

**Fig. 16.** Velocity diagrams for various values of $\phi'$ ($c_u/\gamma B = 0.5$, $D/B = 1$, $q/\gamma B = 0$).

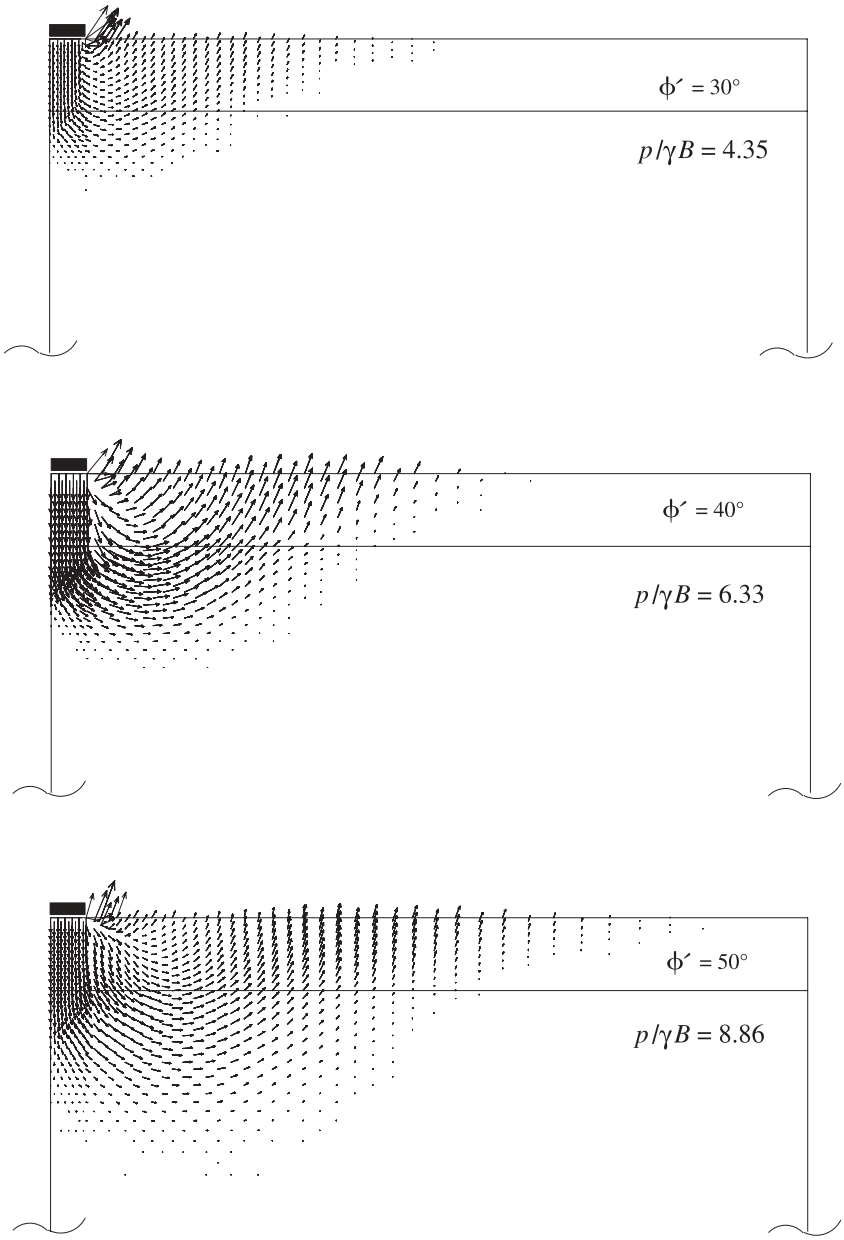


cients and constraints for the mesh, the upper bound formulation of Lyamin and Sloan (2002*b*) leads to a nonlinear programming problem of the form

$$\begin{aligned} &\text{Minimize} \quad \boldsymbol{\sigma}^{\mathrm{T}}\mathbf{B}\mathbf{u} + \mathbf{c}_{\mathrm{u}}^{\mathrm{T}} + \mathbf{c}_{\mathrm{d}}^{\mathrm{T}}\mathbf{d} \quad \text{on} \quad (\mathbf{u},\mathbf{d}) \\ &\text{Subject to} \quad \mathbf{A}_{\mathrm{u}}\mathbf{u} + \mathbf{A}_{\mathrm{d}}\mathbf{d} = \mathbf{b} \\ &\mathbf{B}\mathbf{u} = \sum_{i=1}^{E} \lambda_i \nabla f_i(\boldsymbol{\sigma}) \\ &\lambda_i \geq 0 \quad i = \{1,\ldots E\} \\ &\lambda_i f_i(\boldsymbol{\sigma}) = 0 \quad i = \{1,\ldots E\} \\ &f_i(\boldsymbol{\sigma}) \leq 0 \quad i = \{1,\ldots E\} \\ &\mathbf{d} \geq 0 \end{aligned} \tag{3}$$

where $\mathbf{u}$ is a global vector of unknown velocities; $\mathbf{d}$ is a global vector of unknown discontinuity variables; $\boldsymbol{\sigma}$ is a global vector of unknown element stresses; $\mathbf{c}_{\mathrm{u}}$ and $\mathbf{c}_{\mathrm{d}}$ are vectors of objective function coefficients for the nodal velocities and discontinuity variables, respectively; $\mathbf{A}_{\mathrm{u}}$ and $\mathbf{A}_{\mathrm{d}}$ are matrices of equality constraint coefficients for the nodal velocities and discontinuity variables, respectively; $\mathbf{B}$ is a global matrix of compatibility coefficients that operate on the nodal velocities; $\mathbf{b}$ is a vector of coefficients; $\nabla = \{\partial/\partial\sigma_x, \partial/\partial\sigma_y, \partial/\partial\tau_{xy}\}^{\mathrm{T}}$; $\lambda_i$ is an unknown plastic multiplier rate for element $i$; $f_i$ is the yield function for element $i$; and $E$ is the number of triangular elements. In this equation, the objective function $\boldsymbol{\sigma}^{\mathrm{T}}\mathbf{B}\mathbf{u} + \mathbf{c}_{\mathrm{u}}^{\mathrm{T}}\mathbf{u} + \mathbf{c}_{\mathrm{d}}^{\mathrm{T}}\mathbf{d}$ denotes the total dissipated power, with the first term giving the dissipation in the continuum, the second term giving the dissipation because of fixed boundary tractions or body forces, and the third term giving the dissipation in the discontinuities. Using its

**Fig. 17.** Velocity diagrams for various values of $c_u/\gamma B$ ($\phi' = 40°$, $D/B = 1$, $q/\gamma B = 0$).

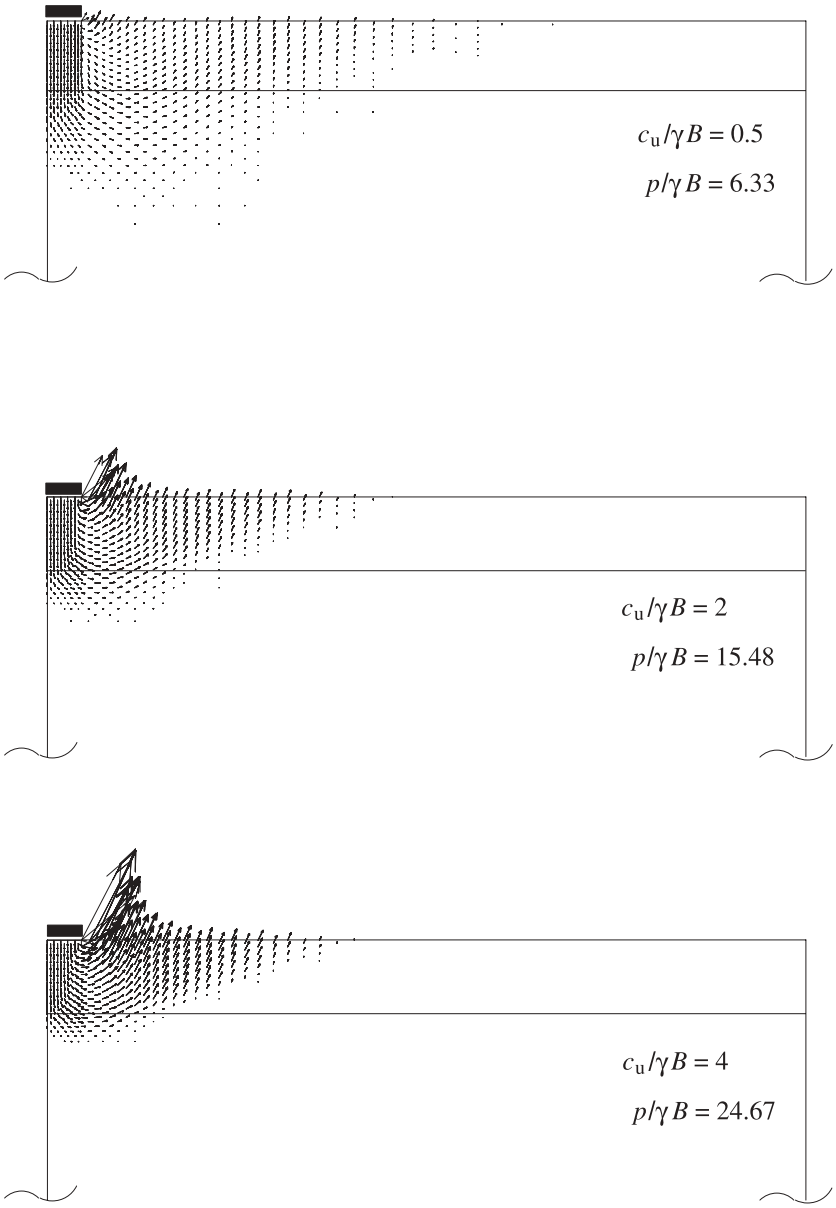


Kuhn-Tucker optimality conditions, the optimization problem (eq. [3]) may be recast in the alternative form

$$\begin{aligned} &\text{Maximize} && \boldsymbol{\sigma}^T\mathbf{B}\mathbf{u} + \mathbf{c}_u^T\mathbf{u} + \mathbf{c}_d^T\mathbf{d} && \text{on} && (\boldsymbol{\sigma}) \\ &\text{Minimize} && \boldsymbol{\sigma}^T\mathbf{B}\mathbf{u} + \mathbf{c}_u^T\mathbf{u} + \mathbf{c}_d^T\mathbf{d} && \text{on} && (\mathbf{u},\mathbf{d}) \\ [4]\quad &\text{Subject to} && \mathbf{A}_u\mathbf{u} + \mathbf{A}_d\mathbf{d} = \mathbf{b} \\ & && f_i(\boldsymbol{\sigma}) \le 0 \quad i = \{1,...E\} \\ & && \mathbf{d} \ge 0 \end{aligned}$$

which has fewer variables (the plastic multipliers are no longer needed) and fewer constraints. The solution to eq. [4] can be computed efficiently using a two-stage quasi-Newton solver which is a variant of the scheme developed for the lower bound method (Lyamin and Sloan 2002*b*). Again, a maximum of 50 iterations is typically required, regardless of the problem size.

Figure 4*b* shows a fan-type mesh for upper bound limit analysis of the problem considered. This mesh is identical to the lower bound mesh in Fig. 4*a*, except it does not need to incorporate extension elements along the bottom and right boundaries. An upper bound solution is obtained by prescribing a unit downward velocity to the nodes on the footing. To model a perfectly rough foundation, these nodes are constrained so that they cannot move horizontally ($u = 0$). After the resulting optimization problem is solved for the imposed boundary conditions, the upper bound on the collapse load is obtained by equating the power expended by the external loads to the power dissipated internally by plastic deformation.

## Results and discussion

Using the methods described in the previous section, finite element limit analyses were performed to obtain upper and

**Fig. 18.** Velocity diagrams for various values of $q/\gamma B$ ($\phi' = 40°$, $c_u/\gamma B = 0.5$, $D/B = 1$).

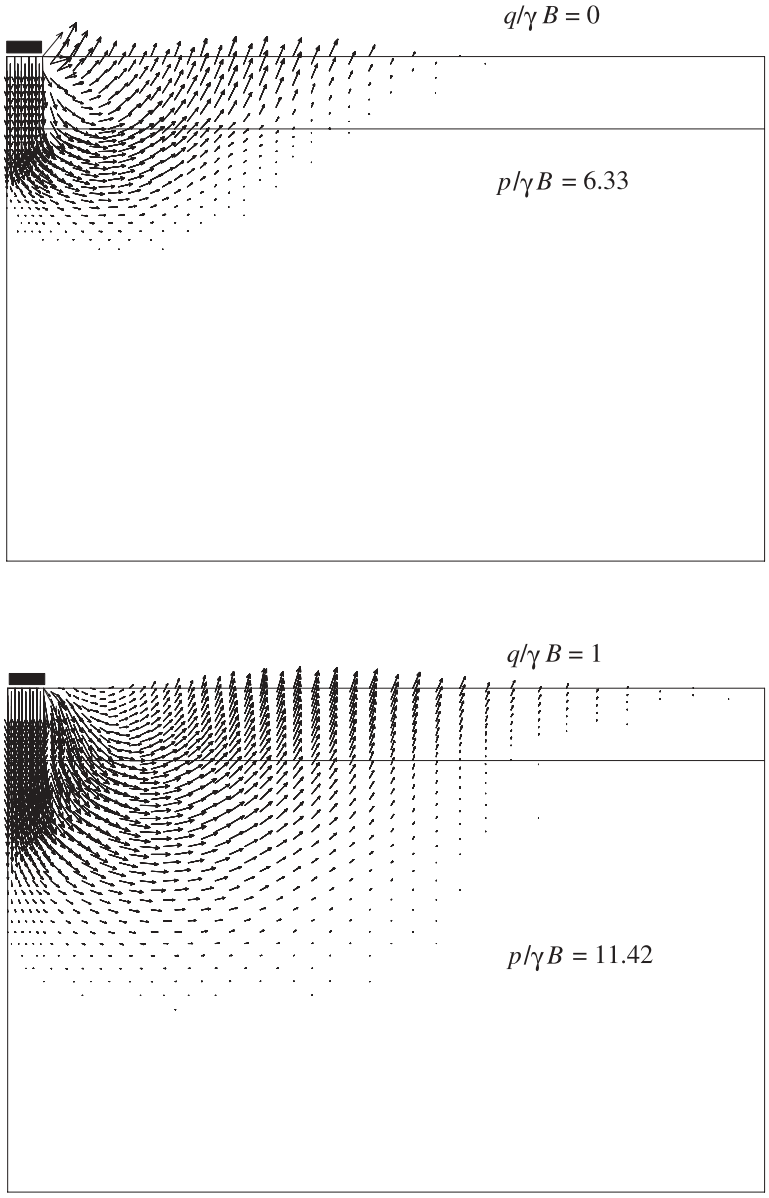


lower bound bearing capacity estimates for strip footings on various sand and clay layers. The study assumes the soil layers obey an associated flow rule and covers a range of parameters, including the depth of the sand layer ($D/B$), the friction angle of the sand ($\phi'$), the undrained shear strength of the clay ($c_u/\gamma B$), and the effect of a surcharge ($q/\gamma B$). The influence of footing roughness and increasing strength with depth for the clay soil are also quantified rigorously. For a single example, the effect of zero dilatancy in the sand layer is investigated approximately by using an associated flow rule with a reduced friction angle. Where possible, the new numerical results are compared with solutions obtained by others.

## Comparisons with previous results

The lower and upper bound estimates of the normalized bearing capacity $p/\gamma B$ are compared with the semi-empirical results suggested by Hanna and Meyerhof (1980), the displacement finite element method solutions of Griffiths (1982) and Burd and Frydman (1996), and the analytical kinematic predictions of Michalowski and Shi (1995). These comparisons are shown in Figs. 7–9. The lower and upper bounds were computed using meshes similar to those in Fig. 4.

For the case of $\phi' = 45°$, $D/B = 2$, and $q/\gamma B = 0$, Fig. 7 shows that the semi-empirical approach of Hanna and Meyerhof (1980) and the analytical kinematic approach of Michalowski and Shi (1995) both overestimate the bearing capacity $p/\gamma B$ at larger values of $c_u/\gamma B$. Although their solutions are reasonably close to our upper bounds, they are up to 18% above our lower bounds. As shown in Fig. 8, the kinematic results of Michalowski and Shi display similar trends for the case of $\phi' = 40°$, $D/B = 1$, and $q/\gamma B = 0$. The numerical results reported by Burd and Frydman (1996),

**Fig. 19.** Effect of footing roughness ($D/B$ = 0.5).

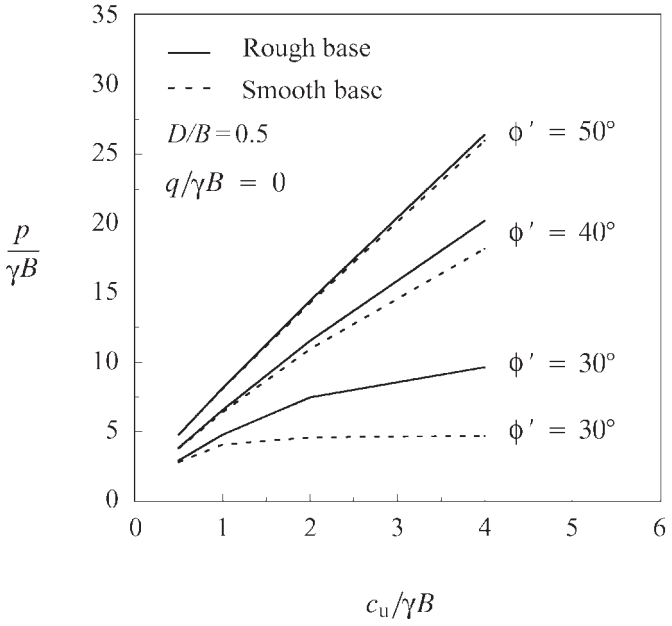


also plotted in Fig. 8, are for a non-associated flow rule with a dilation angle of $\psi' = 10°$ and represent average values obtained from their displacement finite element and finite difference analyses. Their bearing capacity predictions lie close to the average of our upper and lower bound estimates.

To compare their kinematic results with those of Griffiths (1982), who employed the displacement finite element method with a non-associated flow rule for the sand layer, Michalowski and Shi (1995) replace the sand friction angle $\phi'$ by $\overline{\phi'}$, where

$$[5] \qquad \tan\overline{\phi'} = \frac{\cos\psi'\cos\phi'}{1-\sin\psi'\sin\phi'}\tan\phi'$$

This follows the work of Drescher and Detournay (1993) who argue that, for kinematic mechanisms comprised solely of rigid blocks and velocity discontinuities, the use of $\overline{\phi'}$ instead of $\phi'$ will furnish reasonable limit load estimates for materials with coaxial non-associated flow rules. Indeed, Drescher and Detournay suggest that $\overline{\phi'}$ may be viewed as a "residual" friction angle which accounts for the softening that may be induced under certain stress conditions by a non-associated flow rule. Because failure may occur before all the stresses reach the residual state, this approach may give limit loads that are lower than the true values. Figure 9 compares the solutions of Griffiths (1982) and Michalowski and Shi (1995) with our bound solutions for $\overline{\phi'} = 33°$, which approximates the non-associated zero dilation case where $\phi' = 40°$ and $\psi' = 0°$. Since our upper bound method permits plastic dissipation in both the continuum and the velocity discontinuities, and thus violates one of the conditions of the proof by Drescher and Detournay, these results should be treated with some caution. Bearing this in mind, the predictions of Griffiths and Michalowski and Shi are reasonably close to our bound solutions for small to medium values of $c_u/\gamma B$, but give higher bearing capacities as $c_u/\gamma B$ increases.

Because of the large volume changes they predict during plastic shearing, associated flow rules are sometimes thought to give questionable limit loads for frictional soils. For cases where the failure mechanism is kinematically highly constrained, such as granular flow in a hopper, this concern is certainly valid and needs to be addressed. For frictional soils with a freely deforming surface and a semi-infinite domain, however, the use of an associated flow rule will, in many cases, give good estimates of the collapse load. Although difficult to quantify, this important result is discussed at length in Davis (1968) and has been confirmed by a number of independent finite element studies (e.g., Zienkiewicz et al. 1975; Sloan 1981).

Overall, the results shown in Figs. 7–9 suggest that the new bound solutions give bearing capacities which are more conservative than those published previously. Assuming the soil layers obey an associated flow rule, the finite element limit analyses typically bound the limit load to ±10% or better.

## Effect of mesh arrangement

For the case of $\phi' = 40°$, $D/B = 1$, and $q/\gamma B = 0$, Table 1 compares the results from two different types of mesh arrangement with the upper and lower bound analyses. Close bounds are always obtained using mesh type 1 (Fig. 4), which has a fan of discontinuities at the footing edge. The results from mesh type 2 (Fig. 10) are less satisfactory, with the accuracy of the lower bounds decreasing as $c_u/\gamma B$ increases. Solutions from this type of grid cannot be improved by using additional elements, as it will always fail to model the principal stress rotation at the edge of the footing adequately. Interestingly, the accuracy of the upper bound solutions is roughly the same for both types of mesh arrangement. All subsequent limit analysis results in this paper were obtained using fan-type meshes similar to those in Fig. 4.

The central processing unit (CPU) times in Table 1 show that the finite element bound formulations of Lyamin and Sloan (2002*a*, 2002*b*) are computationally very efficient. To obtain solutions of roughly the same accuracy using the conventional displacement method would, in the authors' experience, require similar computational effort. For materials with an associated flow rule, the limit analysis solutions have the key advantage of an built-in error indicator, with the lower bounds always providing a conservative estimate of the bearing capacity. They also furnish the limit load directly, without the need to infer it from a load–deformation response.

## Parametric study

Assuming an associated flow rule for the soil layers, Figs. 11–14 present results for the normalized bearing capacity $p/\gamma B$ as a function of the dimensionless quantities $D/B$, $c_u/\gamma B$, $q/\gamma B$, and $\phi'$. These plots are for $\phi' = 30°$, 40°, and 50°, $q/\gamma B = 0$ and 1, and $D/B = 0.25$, 0.5, 1, and 2 and are averages of the upper and lower bound estimates for the case of a perfectly rough footing. In all cases the spread of the bound solutions is less than ±10%, which is sufficiently accurate for the purposes of design.

**Fig. 20.** Velocity diagrams for rough and smooth footings ($\phi' = 30°$, $c_u/\gamma B = 4$, $D/B = 0.5$, $q/\gamma B = 0$).

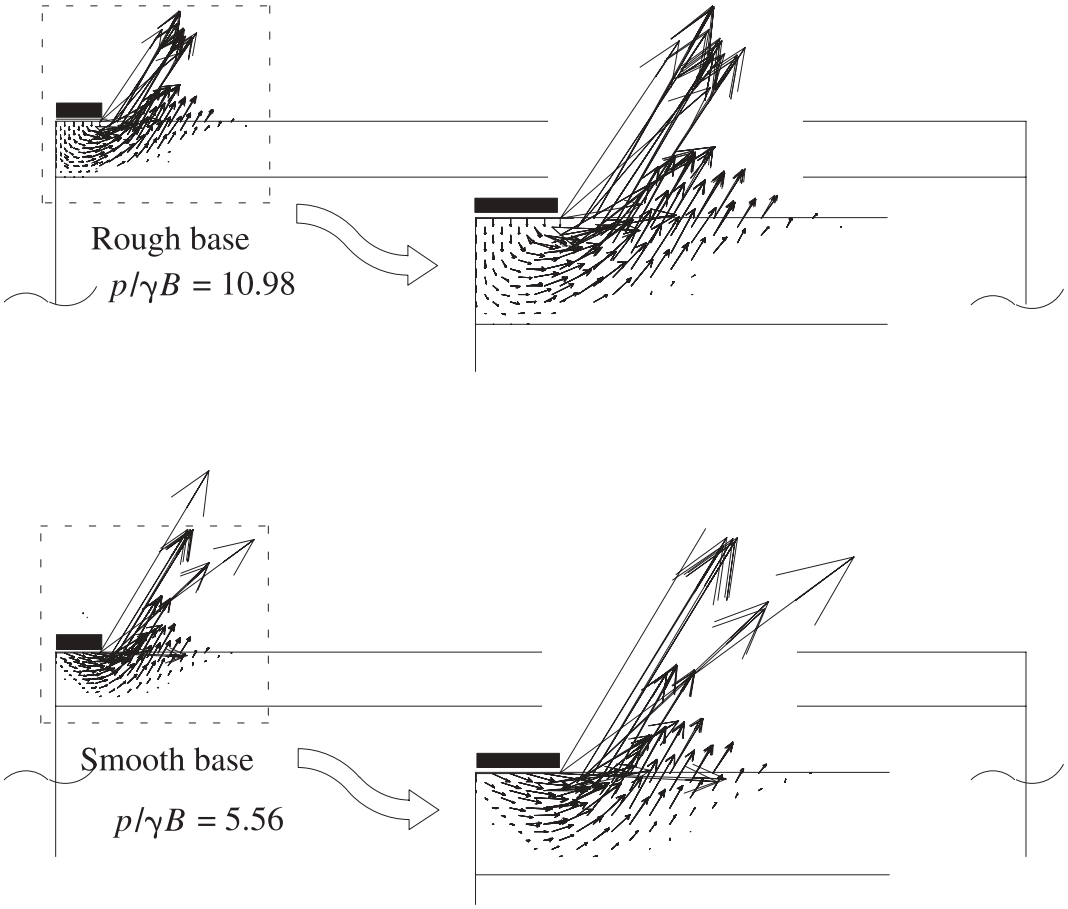


**Fig. 21.** Effect of increasing strength with depth for clay for $D/B = 0.25$.

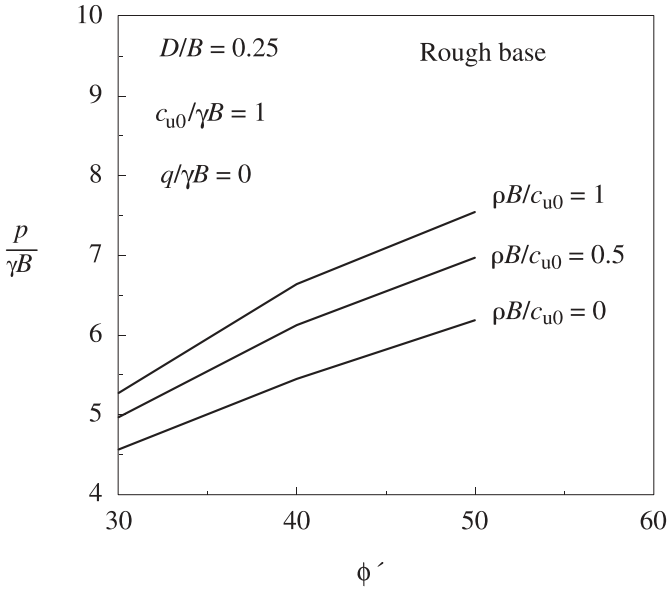


**Fig. 22.** Effect of increasing strength with depth for clay for $D/B = 2$.

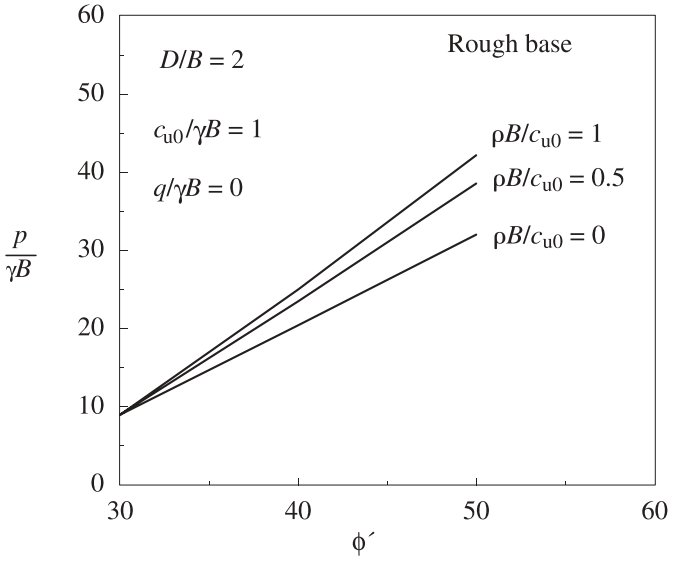


Figure 15 shows the velocity diagrams from the upper bound calculations for various values of $D/B$ with $\phi' = 30°$, $c_u/\gamma B = 1$, and $q/\gamma B = 0$. These plots clearly demonstrate the improved bearing capacity that results from increasing the depth of the sand layer. Note, however, that once $D/B$ exceeds a certain "critical depth" (in this case slightly less than two), the failure mechanism is totally contained within the sand layer and $p/\gamma B$ becomes independent of the shear

**Fig. 23.** Velocity diagrams for various values of $\rho B/c_{u0}$ with $D/B = 0.25$ ($\phi' = 30°$, $c_{u0}/\gamma B = 1$, $q/\gamma B = 0$).

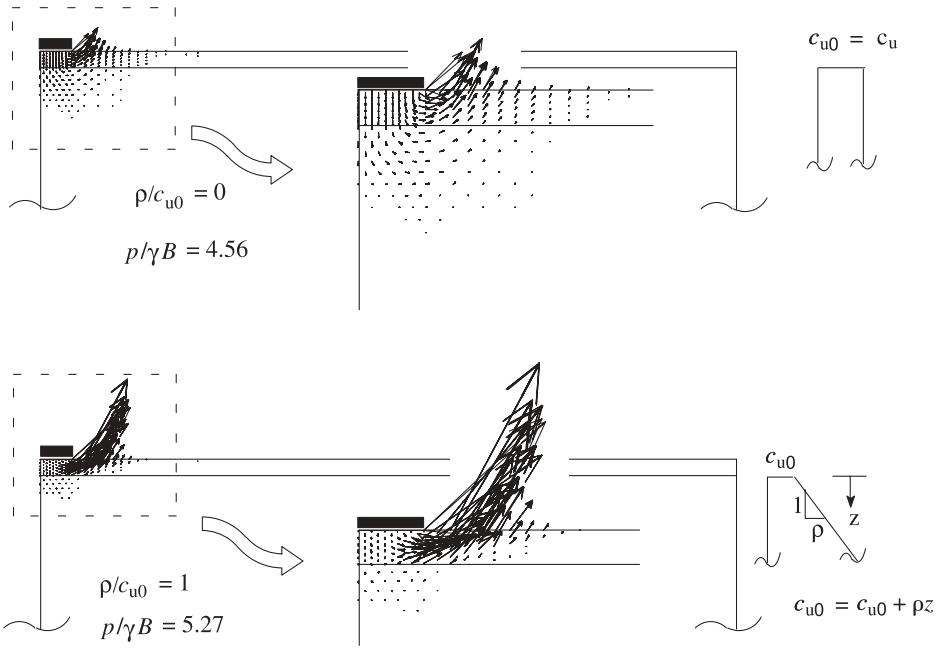


**Fig. 24.** Velocity diagrams for various values of $\rho B/c_{u0}$ with $D/B = 2$ ($\phi' = 30°$, $c_{u0}/\gamma B = 1$, $q/\gamma B = 0$).

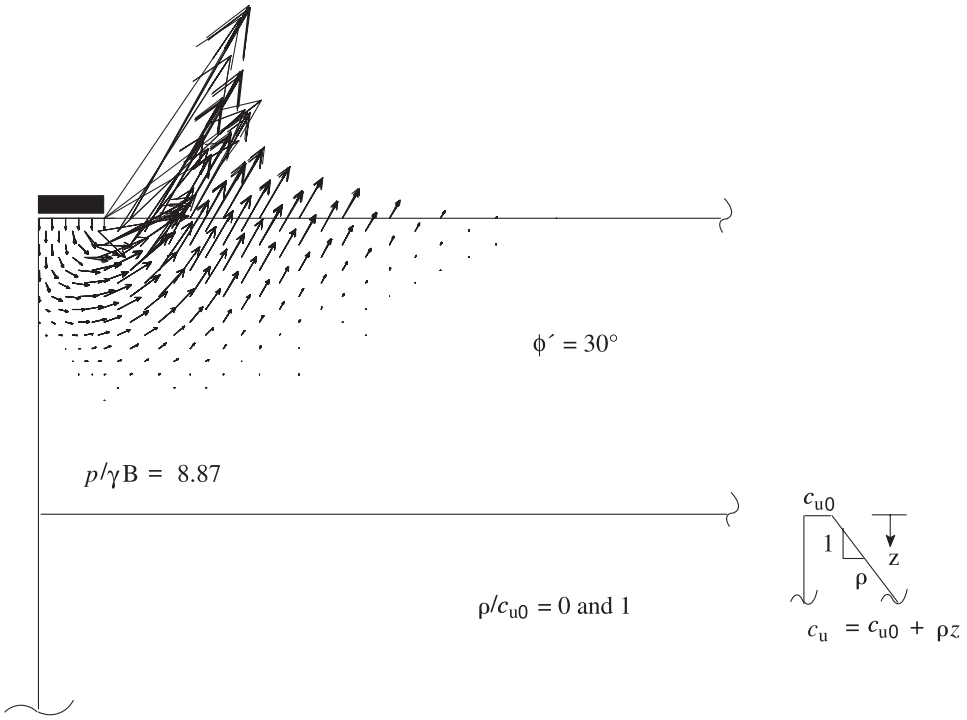


strength of the clay. The existence of this critical depth is clearly evident in Figs. 13 and 14 for the example of $\phi' = 30°$ with no surcharge, where a constant value of $p/\gamma B = 8.87$ is observed. Interestingly, this limiting value is close to the factor $N_\gamma^H/2 = 9.05$ given by Brinch Hansen (1970) but substantially above the factor $N_\gamma^M/2 = 7.83$ predicted by Meyerhof (1951).

As expected, the strength of the sand layer has a greater influence on the bearing capacity for larger values of $D/B$. Considering the case of $c_u/\gamma B = 4$, $D/B = 2$, and $q/\gamma B = 0$, for example, $p/\gamma B$ increases by a factor of 7.75 as $\phi'$ is increased from 30° to 50°. For the same set of strength parameters but with $D/B = 0.25$, this factor is reduced to 1.75. The influence of $\phi'$ on the bearing failure for a sand layer of thickness $D = B$, resting on a soft clay layer with $c_u/\gamma B = 0.5$, is shown

in the velocity plots of Fig. 16. As $\phi'$ increases, the proportion of the failure mechanism in the soft substratum increases, giving rise to the possibility of punching shear failure (Meyerhof 1974).

The effect of the underlying clay strength on the bearing capacity of a sand layer with $\phi' = 40°$ and $D/B = 1$ is illustrated in Fig. 17. Although the bearing capacity increases with increasing $c_u/\gamma B$, its growth is not linearly proportional to this quantity. As expected, the fraction of the failure mechanism confined to the sand layer increases as the undrained shear strength of the clay increases. Indeed, for a fixed $D/B$ and a sufficiently high value of $c_u/\gamma B$, the bearing capacity $p/\gamma B$ would again be governed solely by $\phi'$ and $q/\gamma B$.

Intuitively, we expect a surcharge $q$ to raise the bearing capacity by enlarging the failure mechanism, thus mobilizing more of the available shear strength. This effect is illustrated graphically in Fig. 18 for the case of a footing where $\phi' = 40°$, $c_u/\gamma B = 0.5$, $D/B = 1$, and $q/\gamma B = 0$ or 1. In the latter case, the surcharge clearly suppresses the upward movement of sand near the footing edge and forces the failure mechanism to be much wider and deeper.

**Effect of footing roughness**

As discussed by Chen (1975), approximate estimates for the frictional bearing capacity factor $N_\gamma$ are reduced by a factor of around two when the footing is taken as smooth instead of rough. For the problem considered here, we thus expect this parameter to have the most influence when the bulk of the failure mechanism lies inside the sand layer and there is no surcharge. The average of the upper and lower bounds, shown in Figs. 19 and 20 for $D/B = 0.5$ and $q/\gamma B = 0$, confirms that this is indeed the case, with the biggest difference in bearing capacity occurring for the shallow failure mechanism associated with $\phi' = 30°$and $c_u/\gamma B = 4$. The observed drop in bearing capacity for the smooth footing, which is roughly a factor of two, is consistent with approximate predictions from the Prandtl and Hill mechanisms discussed by Chen. As the friction angle increases, the failure mechanism becomes deeper and wider and the effect of the footing roughness diminishes as the clay influence dominates. In practice, the footing roughness is likely to lie between the perfectly smooth and perfectly rough extremes, with an interface friction angle that is typically one half to two thirds of the sand friction angle. The approximate $N_\gamma$ predictions given by Chen, and the author's independent tests, suggest that the results reported here are largely unaffected for these values.

**Effect of increasing strength with depth for clay**

Soft, normally consolidated clays often exhibit undrained strength profiles that increase linearly with an increase in depth. To investigate the likely influence of this inhomogeneity we assume the undrained strength varies as $c_u(z) = c_{u0} + \rho z$, where $c_{u0}$ is the shear strength at the surface of the clay layer, $z$ is the depth from the surface of the clay layer, and $\rho = dc_u/dz$. Two values of $D/B = 0.25$ and 2 are examined for the case of zero surcharge and a soft clay with $c_{u0}/\gamma B = 1$ and $\rho B/c_{u0} = 0$, 0.5, and 1. The range chosen for $\rho B/c_{u0}$ follows from the field measurements reported in Lambe and Whitman (1979), which suggest that $\rho$ typically varies between 1 and 2 kN/m$^3$ for soft, normally consolidated clay deposits. Figures 21 and 22, which plot the averages of the upper and lower bounds, show that the clay inhomogeneity has the biggest effect on the bearing capacity when $D/B$ is small. This reflects the fact that the failure mechanism extends deeply into the clay bed for shallow sand layers, at least for the range of strength parameters considered here (Fig. 23). In contrast, for a deeper layer of medium-dense sand ($D/B = 2$ and $\phi' = 30°$) on a soft clay ($c_{u0}/\gamma B = 1$), the failure mechanism does not penetrate the underlying deposit and the bearing capacity is unaffected by its properties (Figs. 22, 24).

## Conclusions

The ultimate bearing capacity of a strip footing resting on a sand layer over clay has been investigated using finite element formulations of the classical limit theorems. Rigorous bounds for a wide range of strength and geometry parameters have been obtained, and the effects of footing roughness and clay inhomogeneity studied. Assuming the soil layers obey an associated flow rule, the solutions presented bracket the bearing capacity to within ±10% or better.

## References

Brinch Hansen, J. 1970. A revised and extended formula for bearing capacity. Bulletin of the Danish Geotechnical Institute, **28**: 5–11.

Burd, H.J., and Frydman, S. 1996. Discussion on bearing capacity of footings over two-layered foundation soils. Journal of Geotechnical Engineering, ASCE, **122**(8): 699–700.

Burd, H.J., and Frydman, S. 1997. Bearing capacity of plane-strain footings on layered soils. Canadian Geotechnical Journal, **34**: 241–253.

Chen, W.F. 1975. Limit analysis and soil plasticity. Elsevier, Amsterdam.

Chen, W.F., and Davidson, H.L. 1973. Bearing capacity determination by limit analysis. Journal of the Soil Mechanics and Foundations Division, ASCE, **99**(6): 433–449.

Davis, E.H. 1968. Theories of plasticity and the failure of soil masses. *In* Soil mechanics: selected topics. *Edited by* I.K. Lee. Butterworth, London. pp. 341–380.

Drescher, A., and Detournay, E. 1993. Limit load in translational failure mechanisms for associative and non-associative materials. Géotechnique, **43**(3): 443–456.

Florkiewicz, A. 1989. Upper bound to bearing capacity of layered soils. Canadian Geotechnical Journal, **26**: 730–736.

Griffiths, D.V. 1982. Computation of bearing capacity on layered soil. *In* Proceedings of the 4th International Conference on Numerical Methods in Geomechanics, Edmonton, Alberta, Canada, May. Balkema, Rotterdam, The Netherlands. Vol. 1, pp. 163–170.

Hanna, A.M., and Meyerhof, G.G. 1980. Design charts for ultimate bearing capacity of foundations on sand overlying soft clay. Canadian Geotechnical Journal, **17**: 300–303.

Houlsby, G.T., Milligan, G.W.E., Jewell, R.A., and Burd, H.J. 1989. A new approach to the design of unpaved roads — Part 1. Ground Engineering, **22**(3): 25–29.

Lambe, T.W., and Whitman, R.V. 1979. Soil mechanics. SI version. Wiley, New York.

Lyamin, A.V. 1999. Three-dimensional lower bound limit analysis using nonlinear programming. Ph.D. thesis, University of Newcastle, Callaghan, NSW, Australia.

Lyamin, A.V., and Sloan, S.W. 2002*a*. Lower bound limit analysis using nonlinear programming. International Journal for Numerical Methods in Engineering, **55**: 573–611.

Lyamin, A.V., and Sloan, S.W. 2002*b*. Upper bound limit analysis using linear finite elements and nonlinear programming. International Journal for Numerical and Analytical Methods in Geomechanics, **26**: 181–216.

Merifield, R.S., Sloan, S.W., and Yu, H.S. 1999. Rigorous solutions for the bearing capacity of two layered clay soils. Géotechnique, **49**(4): 471–490.

Meyerhof, G.G. 1951. The ultimate bearing capacity of foundations. Géotechnique, **2**: 301–331.

Meyerhof, G.G. 1974. Ultimate bearing capacity of footings on sand layer overlying clay. Canadian Geotechnical Journal, **11**: 223–229.

Michalowski, R.L., and Shi, L. 1995. Bearing capacity of footings over two-layer foundation soils. Journal of Geotechnical Engineering, ASCE, **121**(5): 421–428.

Nagtegaal, J.C., Parks, D.M., and Rice, J.R. 1974. On numerically accurate finite element solutions in the fully plastic range. Computer Methods in Applied Mechanics and Engineering, **4**: 153–177.

Sloan, S.W. 1981. Numerical analysis of incompressible and plastic solids using finite elements. Ph.D. thesis, University of Cambridge, Cambridge, U.K.

Sloan, S.W. 1988. Lower bound limit analysis using finite elements and linear programming. International Journal for Numerical and Analytical Methods in Geomechanics, **12**: 61–67.

Sloan, S.W. 1989. Upper bound limit analysis using finite elements and linear programming. International Journal for Numerical and Analytical Methods in Geomechanics, **13**: 263–282.

Sloan, S.W., and Kleeman, P.W. 1995. Upper bound limit analysis using discontinuous velocity fields. Computer Methods in Applied Mechanics and Engineering, **127**: 293–314.

Sloan, S.W., and Randolph, M.F. 1982. Numerical prediction of collapse loads using finite element methods. International Journal for Numerical and Analytical Methods in Geomechanics, **6**: 47–76.

Terzaghi, K., and Peck, R.B. 1948. Soil mechanics in engineering practice. 1st ed. John Wiley and Sons, Inc., New York.

Zienkiewicz, O.C., Humpheson, C., and Lewis, R.W. 1975. Associated and nonassociated viscoplasticity and plasticity in soil mechanics. Géotechnique, **25**: 671–689.